Modeling of the Sheet-Molding Process for Poly(methyl methacrylate)

FANGBIN ZHOU,[1] SANTOSH K. GUPTAM,[2,*] AJAY K. RAY[1]

[1] Department of Chemical and Environmental Engineering, National University of Singapore, 10 Kent Ridge Crescent, Singapore 119260

[2] Department of Chemical Engineering, University of Wisconsin, Madison, Wisconsin 53706

Received 3 November 2000; accepted 22 November 2000

ABSTRACT: The sheet-molding process for the production of poly(methyl methacrylate) (PMMA) involves an isothermal batch reactor followed by polymerization in a mold (the latter is referred to as a "sheet reactor"). The temperature at the outer walls of the mold varies with time. In addition, due to finite rates of heat transfer in the viscous reaction mass, spatial temperature gradients are present inside the mold. Further, the volume of the reaction mass also decreases with polymerization. These several physicochemical phenomena are incorporated into the model developed for this process. It was found that the monomer conversion attains high values of near-unity in most of the inner region in the mold. This is because of the high temperatures there, since the heat generated due to the exothermicity of the polymerization cannot be removed fast enough. However, the temperature of the mold walls has to be increased in the later stages of polymerization so that the material near the outer edges can also attain high conversions of about 98%. This would give PMMA sheets having excellent mechanical strength. The effects of important operating (decision) variables were studied and it was observed that the heat-transfer resistance in the mold influences the spatial distribution of the temperature, which, in turn, influences the various properties (e.g., monomer conversion, number-average molecular weight, and polydispersity index) of the product significantly. © 2001 John Wiley & Sons, Inc. J Appl Polym Sci 81: 1951–1971, 2001

Key words: poly(methyl methacrylate); sheet-reactor; sheet-molding; modeling; polymer reactor

INTRODUCTION

Poly(methyl methacrylate) (PMMA) is a major commodity plastic. An important application of PMMA stems from its transparency, and it is used as a replacement of glass. Even though large-scale sheet molding of PMMA has been carried out for several decades,[1] more art than science is involved in this operation. Very little work has been reported in the open literature on the modeling and simulation of this process. In the last two decades, a considerable amount of knowledge has become available on the modeling of the bulk polymerization of methyl methacrylate (MMA). In this article, this knowledge is extended to model the *industrial* process of the sheet molding of PMMA.

A distinguishing feature of the bulk polymerization of MMA is the presence of an extremely strong Trommsdorff[2,3] effect. This is a manifesta-

Correspondence to: A. K. Ray (cheakr@nus.edu.sg).
*On leave from the Indian Institute of Technology, Kanpur, 208016, India.

Journal of Applied Polymer Science, Vol. 81, 1951–1971 (2001)

Table I Kinetic Scheme for Bulk-addition Polymerization of MMA

Initiation	$I \xrightarrow{(f)k_d} 2R$
	$R + M \xrightarrow{k_i} P_1$
Propagation	$P_n + M \xrightarrow{k_p} P_{n+1}$
Termination (disproportionation)	$P_n + P_m \xrightarrow{k_t} D_n + D_m$

tion of the significant decrease of the apparent rate constants (see Table I), k_t and k_p, as well as the initiator efficiency, f, at monomer conversions above about 40%. This is because the viscosity of the reaction mass increases significantly and diffusional limitations assume considerable significance under these conditions. Excellent models[4–7] for this effect have appeared in the last few years and have been reviewed recently.[8,9] These can now be applied to simulate large-scale operations where physicochemical effects like heat and mass transfer are involved, in addition to chemical re-

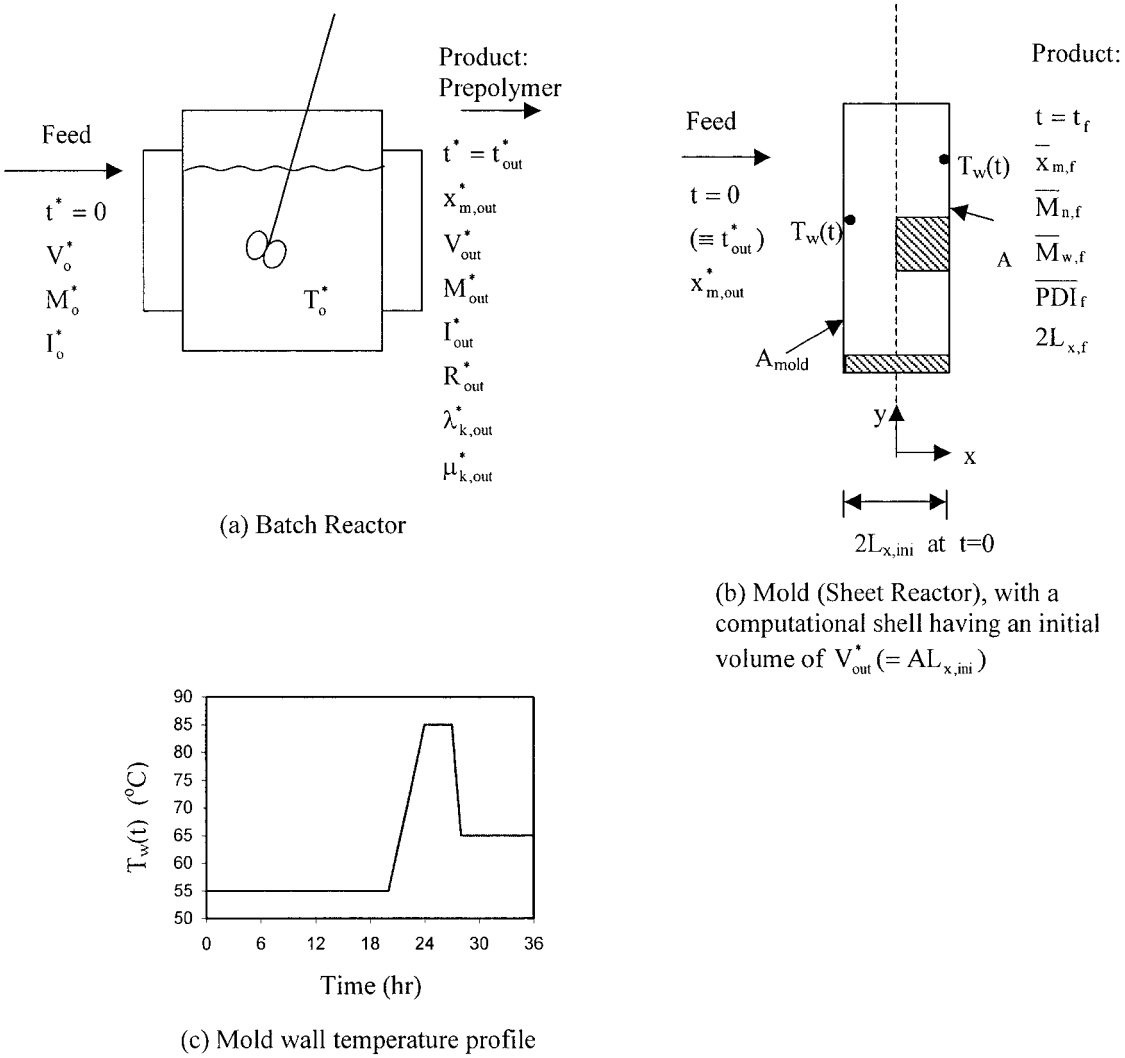

Figure 1 Schematic diagram of the sheet-molding process for PMMA: (a) batch reactor; (b) mold (sheet reactor), with a repeating computational shell having a volume $V^*_{\text{out}} = AL_{x,\text{ini}}$; (c) wall-temperature history in the sheet reactor commonly used in industry.[1]

Table II Equations for the Batch Reactor

$$\frac{dI^*}{dt} = -k_d I^*$$

$$\frac{dM^*}{dt} = -k_p \frac{\lambda_0^* M^*}{V^*} - k_i \frac{R^* M^*}{V^*}$$

$$\frac{dR^*}{dt} = 2fk_d I^* - k_i \frac{R^* M^*}{V^*}$$

$$\frac{d\lambda_0^*}{dt} = k_i \frac{R^* M^*}{V^*} - k_t \frac{\lambda_0^* \lambda_0^*}{V^*}$$

$$\frac{d\lambda_1^*}{dt} = k_i \frac{R^* M^*}{V^*} + k_p \frac{\lambda_0^* M^*}{V^*} - k_t \frac{\lambda_0^* \lambda_1^*}{V^*}$$

$$\frac{d\lambda_2^*}{dt} = k_i \frac{R^* M^*}{V^*} + k_p M^* \frac{(\lambda_0^* + 2\lambda_1^*)}{V^*} - k_t \frac{\lambda_0^* \lambda_2^*}{V^*}$$

$$\frac{d\mu_0^*}{dt} = k_t \frac{\lambda_0^{*2}}{V^*}$$

$$\frac{d\mu_1^*}{dt} = k_t \frac{\lambda_0^* \lambda_1^*}{V^*}$$

$$\frac{d\mu_2^*}{dt} = k_t \frac{\lambda_0^* \lambda_2^*}{V^*}$$

$$P^* = (M_0^* - M^*)(\mathrm{MW}_m)$$

Initial conditions (I.C.); $t^* = 0$: choose V_0^* arbitrarily. $I^* = I_0^* = [I_0]^* V_0^*$; $M^* = M_0^* = \rho_m(T_0^*)V_0^*/(\mathrm{MW}_m)$; R^*, $\lambda_{k,0}^*$, $\mu_{k,0}^*(k = 0, 1, 2) = 0$.

action. The sheet molding of PMMA is an example which is modeled in this work.

In this process (see Fig. 1), a volume, V_0^*, of a mixture of M_0^* mol of MMA and I_0^* mol of the initiator (AIBN) is first polymerized in a well-stirred, isothermal (T_0^*) batch reactor. A volume, T_{out}^*, of the product prepolymer is obtained. The monomer conversion in the batch reactor is $x_{\mathrm{m,out}}^*$, and the total reaction time is T_{out}^*. This mixture is then filled into the mold. The latter is a thin hollow box, the faces of which are formed of two *large* parallel glass sheets (each of area A_{mold}), separated by a distance of $2L_{x,\mathrm{ini}}$ by the use of thin strips of *compressible* material (spacers). Further polymerization of the reaction mass takes place in the completely filled mold as it passes through a temperature-programmed oven. The temperature, $T_w(t)$, of the outer surfaces of the reaction mass is assumed to be a function of time, t. Beattie[1] gave the typical temperature history used in industry [Fig. 1(c)]. The elastic spacers become compressed as polymerization takes place in the mold, to accommodate the contraction in the volume of the reaction mixture. A computer model is first developed for the polymerization of MMA in the mold, to study the effect of the nonisothermal temperature history on the variation of the monomer conversion and of the average molecular weights of the polymer during this process.

FORMULATION

The sheet-molding process for PMMA as described above is now modeled. The process, shown schematically in Figure 1, involves two reactors, namely, a batch reactor followed by a "sheet" reactor. The polymerization in the isothermal batch reactor was modeled and extensively studied earlier.[7,10–13] Table II summarizes the mass balance and moment equations describing this reactor. The change in the volume during polymerization

Table III Cage, Gel, and Glass-effect Equations for Bulk Polymerizations[7]

$$\frac{1}{f} = \frac{1}{f_0}\left[1 + \theta_f(T)\frac{M}{V}\frac{1}{\exp[\xi_{\mathrm{I3}}\{-\psi + \psi_{\mathrm{ref}}\}]}\right] \quad (1)$$

$$\frac{1}{k_t} = \frac{1}{k_{t,0}} + \theta_t(T)\mu_n^2\frac{\lambda_0}{V}\frac{1}{\exp[-\psi + \psi_{\mathrm{ref}}]} \quad (2)$$

$$\frac{1}{k_p} = \frac{1}{k_{p,0}} + \theta_p(T)\frac{\lambda_0}{V}\frac{1}{\exp[\xi_{13}\{-\psi + \psi_{\mathrm{ref}}\}]} \quad (3)$$

$$\psi = \frac{\gamma\left\{\dfrac{\rho_m\phi_m\hat{V}_m^*}{\xi_{13}} + \rho_p\phi_p\hat{V}_p^*\right\}}{\rho_m\phi_m\hat{V}_m^*V_{fm} + \rho_p\phi_p\hat{V}_p^*V_{fp}} \quad (4)$$

$$\psi_{\mathrm{ref}} = \frac{\gamma}{V_{fp}} \quad (5)$$

$$V = \frac{M^*(\mathrm{MW}_m)}{\rho_m(T_0^*)} + \frac{P^*}{\rho_p(T_0^*)}\ (\text{batch}); \quad V_{j,\mathrm{new}}(t)\ (\text{in Table V})\ (\text{sheet}) \quad (6)$$

$$\phi_m = \frac{M^*(\mathrm{MW}_m)/\rho_m(T_0^*)}{\dfrac{M^*(\mathrm{MW}_m)}{\rho_m(T_0^*)} + \dfrac{(M_0^* - M^*)(\mathrm{MW}_m)}{\rho_p(T_0^*)}}\ (\text{batch}); \quad \phi_{m,j,\mathrm{new}}(t)\ (\text{in Table V})\ (\text{sheet}) \quad (7)$$

$$\phi_p = 1 - \phi_m \quad (8)$$

$$\xi_{13} = \frac{\hat{V}_m^*(\mathrm{MW}_m)}{\hat{V}_p^* M_{jp}} \quad (9)$$

$$\xi_{\mathrm{I3}} = \frac{\hat{V}_I^*(\mathrm{MW}_I)}{\hat{V}_p^* M_{jp}} \quad (10)$$

$$k_d = k_d^0\exp(-E_d/R_gT) \quad (11)$$

$$k_{p,0} = k_{p,0}^0\exp(-E_p/R_gT) \quad (12)$$

$$k_{t,0} = k_{t,0}^0\exp(-E_t/R_gT) \quad (13)$$

Variables with a superscript * are used for the batch reactor; variables with subscript j are used for the sheet reactor ($j = 1, 2, \ldots, N$).

Table IV Parameters Used for Bulk Polymerization of MMA with AIBN[7,14–16]

$\rho_m = 966.5 - 1.1[T(\mathrm{K}) - 273.15]$ kg/m^3
$\eta_p = 1200$ kg/m^3
$f_0 = 0.58$
$k_d^0 = 1.053 \times 10^{15}$ s^{-1}
$k_{p,0}^0 = 4.917 \times 10^2$ m^3 mol^{-1} s^{-1}
$k_{t,0}^0 = 9.8 \times 10^4$ m^3 mol^{-1} s^{-1}
$k_i = k_p$
$E_d = 128.45$ kJ/mol
$E_p = 18.22$ kJ/mol
$E_t = 2.937$ kJ/mol
$(\mathrm{MW}_m) = 0.10013$ kg/mol
$(\mathrm{MW}_I) = 0.06800$ kg/mol

Parameters for the cage, gel, and glass effects[7]

$\hat{V}_I^* = 9.13 \times 10^{-4}$ m^3/kg
$\hat{V}_m^* = 8.22 \times 10^{-4}$ m^3/kg
$\hat{V}_p^* = 7.70 \times 10^{-4}$ m^3/kg
$M_{jp} = 0.18781$ kg/mol
$\gamma = 1$
$V_{fm} = 0.149 + 2.9 \times 10^{-4}\ [T(\mathrm{K}) - 273.15]$
$V_{fp} = 0.0194 + 1.3 \times 10^{-4}\ [T(\mathrm{K}) - 273.15 - 105]$

Correlations used for the θ's[7]

$\log_{10}[\theta_t(T), s] = a_1 - a_2(1/T) + a_3(1/T^2)$
$\log_{10}[\theta_p(T), s] = b_1 - b_2(1/T) + b_3(1/T^2)$
$\log_{10}[10^3\theta_f(T), \mathrm{m}^3\ \mathrm{mol}^{-1}] = c_1 - c_2(1/T) + c_3(1/T^2)$
$a_1 = 1.2408 \times 10^2$; $a_2 = 1.0314 \times 10^5$; $a_3 = 2.2735 \times 10^7$
$b_1 = 8.0300 \times 10^1$; $b_2 = 7.5000 \times 10^4$; $b_3 = 1.7650 \times 10^7$
$c_1 = 2.0160 \times 10^2$; $c_2 = 1.4550 \times 10^5$; $c_3 = 2.7000 \times 10^7$

Parameters for the sheet reactor[14–16]

$C_{p,\mathrm{mix}} = 1.674$ kJ kg^{-1} K^{-1}
$\Delta H_r = -58.19$ kJ/mol
$K_T = 0.13$ W m^{-1} K^{-1}
$\rho_{\mathrm{mix},j}(t) = \dfrac{M_{j,\mathrm{new}}(t)(\mathrm{MW}_m) + P_{j,\mathrm{new}}(t)}{V_{j,\mathrm{new}}(t)}$
$A = V_{\mathrm{out}}^*/L_{x,\mathrm{ini}}$; (independent of time)
$V_{\mathrm{out}}^* = 0.0065$ m^3

is accounted for, since the volume, V^*, at any time, t^*, is computed as the sum of the volumes of the unreacted monomer present and that of the polymer produced until that time. A new variable, $P^*(t^*)$, is defined in this table. This is the total mass (kg) of the polymer produced until time t^* in the batch reactor. Tracking of this variable in the sheet reactor (described later) makes it easy to evaluate the *local* values of the monomer conversion. Table III presents the equations for the rate constants and the initiator efficiency, f, in the presence of diffusional limitations, while Table IV gives the values of all the parameters used. These tables provide the same information as given by Seth and Gupta[7] and so the details are not repeated here. These stiff ordinary differential equations[17] (ODEs) are integrated from $t^* = 0$, using the subroutine DIVPAG, in the IMSL library, for the given conditions (T_0^*, V_0^*, and $[I_0]^*$ etc.; M_0^* being computed from V_0^* and T_0^*). The value of the parameter, TOL, used in the code DIVPAG was 10^{-6}. The integration is continued

Table V Equations for the Sheet Reactor, $t \le$ time $\le t + \Delta t$

PDEs

$$\frac{\partial I}{\partial t} = -k_d I$$

$$A(\Delta x)\frac{\partial M}{\partial t} = -k_p M\lambda_0 - k_t MR$$

$$A(\Delta x)\frac{\partial R}{\partial t} = 2fk_d I(A\Delta x) - k_t RM$$

$$A(\Delta x)\frac{\partial \lambda_0}{\partial t} = k_t RM - k_t\lambda_0^2$$

$$A(\Delta x)\frac{\partial \lambda_1}{\partial t} = k_t RM + k_p\lambda_0 M - k_t\lambda_0\lambda_1$$

$$A(\Delta x)\frac{\partial \lambda_2}{\partial t} = k_t RM + k_p M(\lambda_0 + 2\lambda_1) - k_t\lambda_0\lambda_2$$

$$A(\Delta x)\frac{\partial \mu_0}{\partial t} = k_t\lambda_0^2$$

$$A(\Delta x)\frac{\partial \mu_1}{\partial t} = k_t\lambda_0\lambda_1$$

$$A(\Delta x)\frac{\partial \mu_2}{\partial t} = k_t\lambda_0\lambda_2$$

$$\frac{\partial}{\partial t}(\rho_{\text{mix}}C_{p,\text{mix}}T) = K_T\frac{\partial^2 T}{\partial x^2} + (-\Delta H_r)\frac{k_p M\lambda_0}{[A(\Delta x)]^2}$$

"Initial" conditions at time t (after redistribution of grid planes in the previous time interval); $j = 1, 2, \ldots, N$, at time t; known (from previous computation):

$I_{j,\text{new}}(t)$; $M_{j,\text{new}}(t)$; $R_{j,\text{new}}(t)$; $\lambda_{k,j,\text{new}}(t)$, $\mu_{k,j,\text{new}}(t)$; $k = 0, 1, 2$

$T_{j,\text{new}}(t)$; $P_{j,\text{new}}(t)$;

$\Delta x_{j,\text{new}}(t) = L_x(t)/N$; $V_{j,\text{new}}(t) = A[\Delta x_{j,\text{new}}(t)]$

$$\phi_{m,j,\text{new}}(t) = \frac{M_{j,\text{new}}(t)(\text{MW}_m)}{\rho_m[T_{j,\text{new}}(t)]}\Big/V_{j,\text{new}}(t)$$

(Special case; at $t = 0$, use all moles as $(1/N) \times$ (output value from batch reactor) and all T_j as T_0^*).

Boundary conditions (BCs):

at $x = 0$(center):

$$\frac{\partial T}{\partial x} = 0$$

at $x = L_x(t)$(wall):

$0 \le t \le 20$ h, $T_{\text{wall}} = 55$°C

20 h $\le t \le$ 24 h, $T_{\text{wall}} = 55 + 7.5(t - 20)$°C

24 h $\le t \le$ 27 h, $T_{\text{wall}} = 85$°C

27 h $\le t \le$ 28 h, $T_{\text{wall}} = 85 - 20(t - 27)$°C

28 h $\le t \le$ 36 h, $T_{\text{wall}} = 65$°C

Table V *Continued*

Integrate PDEs after converting to ODE–IVPs using DSS002, from t to $t + \Delta t$, to give

$I_j(t + \Delta t)$; $M_j(t + \Delta t)$; $R_j(t + \Delta t)$; $\lambda_{k,j}(t + \Delta t)$; $(k = 0, 1, 2)$; $\mu_{k,j}(t + \Delta t)$; $(k = 0, 1, 2)$; $T_j(t + \Delta t)$;

Then:

$$P_j(t + \Delta t) = P_j(t) + [M_j(t) - M_j(t + \Delta t)](\text{MW}_m)$$

$$V_j(t + \Delta t) = \frac{M_j(t + \Delta t)(\text{MW}_m)}{\rho_m[T_j(t + \Delta t)]} + \frac{P_j(t + \Delta t)}{\rho_p[T_j(t + \Delta t)]}$$

$$\Delta x_j(t + \Delta t) = V_j(t + \Delta t)/A$$

$$L_x(t + \Delta t) = \sum_{j=1}^{N}\Delta x_j(t + \Delta t)$$

Redistribute grid planes *instantaneously* at $t + \Delta t$:

$\Delta x_{j,\text{new}}(t + \Delta t) = L_x(t + \Delta t)/N$

- Plot

$I_j(t + \Delta t)/V_j(t + \Delta t)$; $M_j(t + \Delta t)/V_j(t + \Delta t)$; $R_j(t + \Delta t)/V_j(t + \Delta t)$; $\lambda_{k,j}(t + \Delta t)/V_j(t + \Delta t)$; $\mu_{k,j}(t + \Delta t)/V_j(t + \Delta t)$; $T_j(t + \Delta t)$; $P_j(t + \Delta t)/V_j(t + \Delta t)$;

as functions of x (center points of each finite-difference cell to be used for plotting value for j^{th} cell); see Figure A

- Connect by smooth curves
- Read off values on smooth curves at equispaced locations, $x_{j,\text{new}}$:

$$x_{j,\text{new}}(t + \Delta t) = \frac{L_x(t + \Delta t)}{N} \times \frac{2j + 1}{2};$$

$j = 0, 1, \ldots (N - 1)$ (See Fig. A)

- Multiply all the interpolated concentrations (not the temperature) by appropriate $V_{j,\text{new}}(t + \Delta t) = A \times \Delta x_{j,\text{new}}(t + \Delta t)$
- Gives: $T_{j,\text{new}}(t + \Delta t)$ as well as $I_{j,\text{new}}(t + \Delta t)$; $M_{j,\text{new}}(t + \Delta t)$; $R_{j,\text{new}}(t + \Delta t)$; $\lambda_{k,j,\text{new}}(t + \Delta t)$; $(k = 0, 1, 2)$; $\mu_{k,j,\text{new}}(t + \Delta t)$; $(k = 0, 1, 2)$; $P_{j,\text{new}}(t + \Delta t)$

until the monomer conversion reaches the desired value, x_{out}^*, at which time $t^* = T_{\text{out}}^*$ This code provides the composition and volume of the prepolymer that is fed into the mold.

The prepolymer is poured into the mold at time T_{out}^*. We redefine the time, t (*all* the variables in the sheet reactor are used *without* the superscript *), in this reactor, to start from $t = 0$. Thus, $t = 0$ in this sheet reactor is identical to $t^* = T_{\text{out}}^*$ in the batch reactor. The initial thickness of the mold is $2L_{x,\text{ini}}$. The symmetry of the sheet reactor is now

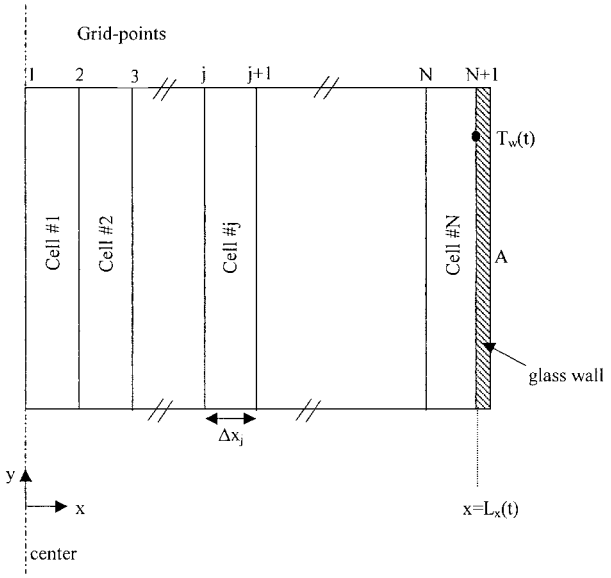

Figure 2 Finite-difference grid planes in the repeating computational shell in the sheet reactor.

exploited. It is assumed that the volume, V^*_{out}, of the prepolymer from the batch reactor fills only a (repeating) part of the mold, shown as the shaded region in Figure 1(b). This corresponds to a cross-sectional area, A ($\ll A_{mold}$), of each glass plate. In fact, the volume, V^*_0, of the *initial* mixture taken in the batch reactor can be selected somewhat arbitrarily, and the area, A, of the sheet reactor corresponding to the associated prepolymer (of volume V^*_{out}) can be *computed*. This area, A, forms a *repeating* "computational cell" (of volume $AL_{x,ini} = V^*_{out}$). What occurs in one such computational

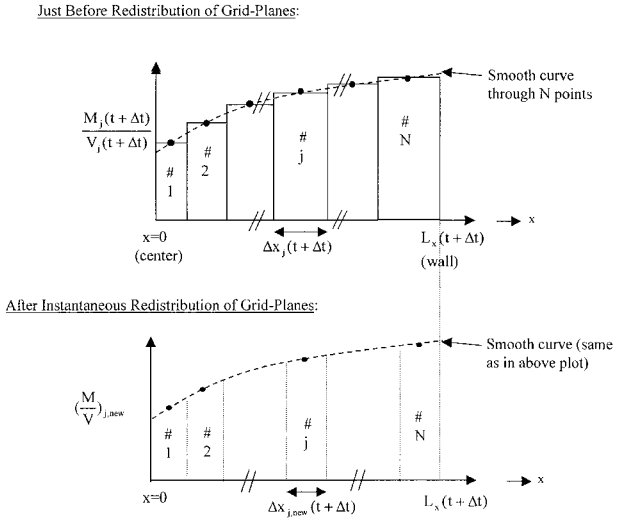

Figure A Interpolation procedure (example of *M*/*V*).

Table VI Equations for Monomer Conversion, Average Molecular Weights, and PDI

Batch reactor

At any time, t^*; $0 \le t^* \le t^*_{out}$

$$x^*_m = (M^*_0 - M^*)/M^*_0$$

$$M^*_n = (\mathrm{MW}_m)\frac{\lambda^*_1 + \mu^*_1}{\lambda^*_0 + \mu^*_0}$$

$$M^*_w = (\mathrm{MW}_m)\frac{\lambda^*_2 + \mu^*_2}{\lambda^*_1 + \mu^*_1}$$

$$\mathrm{PDI}^* = \frac{M^*_w}{M^*_n}$$

Sheet reactor

At time t; $0 \le t \le t_f$; [values *after* redistribution of grid planes]

Local values:

$$M^{**}_{0,j} = M_{j,\mathrm{new}}(t+\Delta t) + \frac{P_{j,\mathrm{new}}(t+\Delta t)}{(\mathrm{MW}_m)}$$

$$x_{m,j,\mathrm{new}}(t+\Delta t) = 1 - \frac{M_{j,\mathrm{new}}(t+\Delta t)}{M^{**}_{0,j}}$$

$$M_{n,j,\mathrm{new}}(t+\Delta t) = \frac{(\lambda_1+\mu_1)_{j,\mathrm{new}}(t+\Delta t)}{(\lambda_0+\mu_0)_{j,\mathrm{new}}(t+\Delta t)}$$

$$M_{w,j,\mathrm{new}}(t+\Delta t) = \frac{(\lambda_2+\mu_2)_{j,\mathrm{new}}(t+\Delta t)}{(\lambda_1+\mu_1)_{j,\mathrm{new}}(t+\Delta t)}$$

$$\mathrm{PDI}_{j,\mathrm{new}}(t+\Delta t) = \frac{M_{w,j,\mathrm{new}}(t+\Delta t)}{M_{n,j,\mathrm{new}}(t+\Delta t)}$$

Cross-section average values:

$$\bar{x}_{m,\mathrm{new}}(t+\Delta t) = \frac{M^*_0 - \sum_{j=1}^{N} M_{j,\mathrm{new}}(t+\Delta t)}{M^*_0}$$

$$\bar{M}_{n,\mathrm{new}}(t+\Delta t) = (\mathrm{MW}_m)\frac{\sum_{j=1}^{N}(\lambda_1+\mu_1)_{j,\mathrm{new}}(t+\Delta t)}{\sum_{j=1}^{N}(\lambda_0+\mu_0)_{j,\mathrm{new}}(t+\Delta t)}$$

$$\bar{M}_{w,\mathrm{new}}(t+\Delta t) = (\mathrm{MW}_m)\frac{\sum_{j=1}^{N}(\lambda_2+\mu_2)_{j,\mathrm{new}}(t+\Delta t)}{\sum_{j=1}^{N}(\lambda_1+\mu_1)_{j,\mathrm{new}}(t+\Delta t)}$$

$$\overline{\mathrm{PDI}}_{\mathrm{new}}(t+\Delta t) = \frac{\bar{M}_{w,\mathrm{new}}(t+\Delta t)}{\bar{M}_{n,\mathrm{new}}(t+\Delta t)}$$

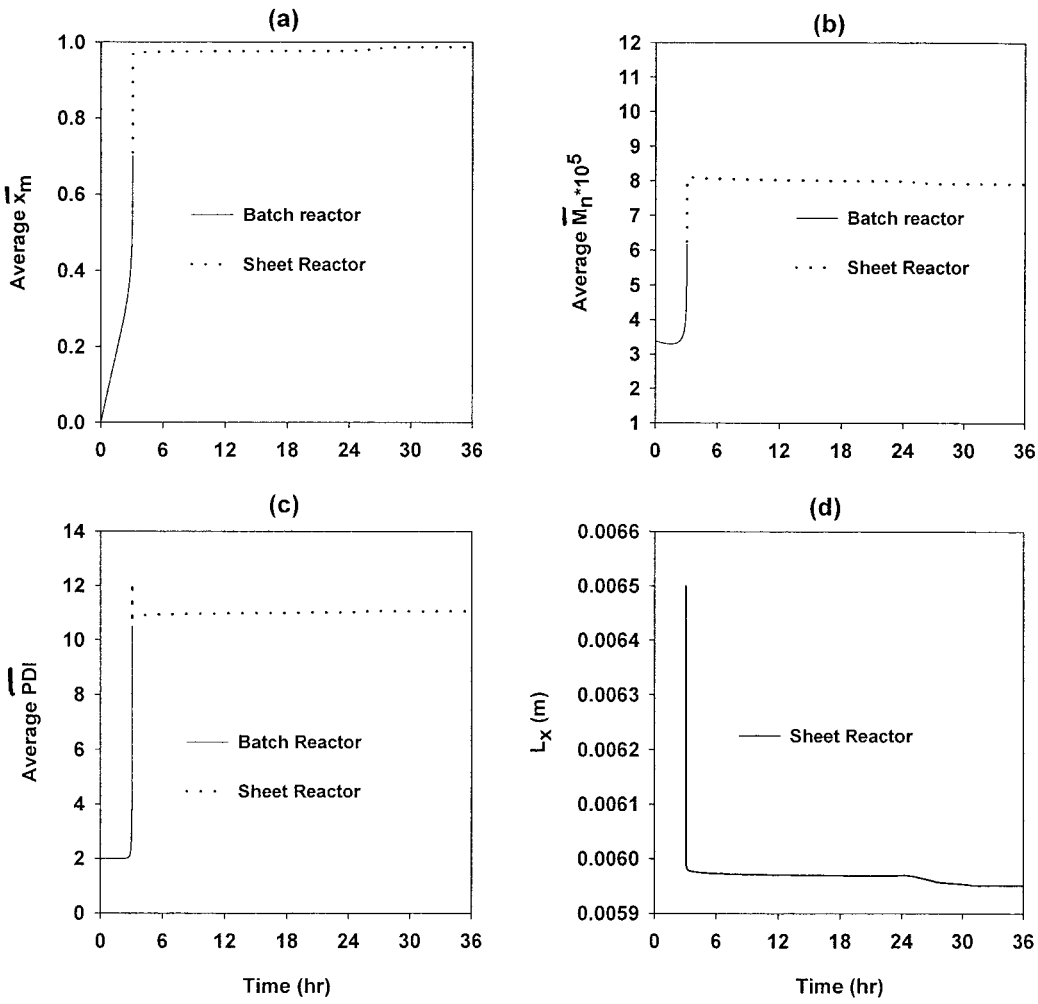

Figure 3 Section-average values of $\bar{x}_m$, $\bar{M}_n$, and $\overline{\text{PDI}}$, and half the sheet thickness, L_x, as a function of time, t, for the reference conditions . Solid lines represent the batch reactor while dotted lines represent the sheet reactor.

cell is duplicated in other similar cells in the mold (assuming that the end effects are negligible). Thus, the solution for a single computational cell gives information about the entire mold. This computational repeating cell is somewhat akin to a unit cell in a crystal.

Equations representing the mass balance, moments, and energy balance for the repeating computational cell in the sheet reactor can easily be written. These equations must account for the heat transfer through the viscous reaction mass in the transverse (x) direction. The temperature, T, as well as the concentrations of all species and moments in this cell would be functions of both the time, t, as well as the location, x. No variation is expected for any variable in the y- and z-directions (complete symmetry in these two directions is assumed). The equations describing the polymerization in the computational cell are, therefore, partial differential equations (PDEs).

The PDEs describing the polymerization in a computational cell in the sheet reactor are of the following form (see Table V):

$$\partial \mathbf{x}/\partial t = \mathbf{f}(\mathbf{x}, \partial^2 \mathbf{x}/\partial \mathbf{x}^2, \mathbf{u}) \tag{1a}$$

$$x_i(t = 0) = x^*_{i,\text{out}};\ i = 1, 2, \ldots, 9;\ x_{10}(t = 0) = T^*_0 \tag{1b}$$

$$T[x = L_x(t)] = T_w(t) \tag{1c}$$

$$\partial T/\partial y(x = 0) = 0 \tag{1d}$$

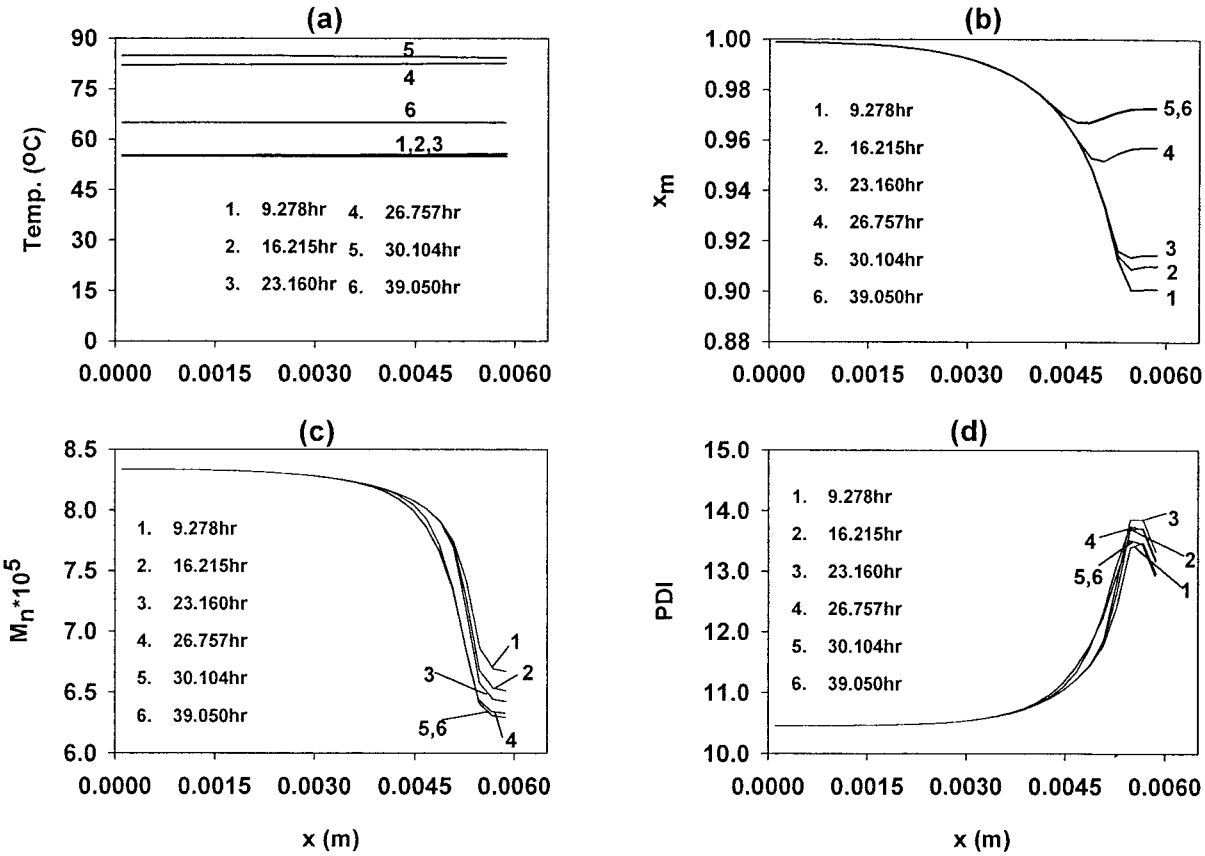

Figure 4 Variation of the local values of the temperature (T), x_m, M_n, and PDI in the sheet reactor, as a function of x at different times. $x = 0$ represents the center plane in the mold. Values of the decision variables are those for the reference case . The temperature profiles for $t \leq 20$ h are the same as in Figure 6(a) [$T_w(t)$ being the same for these two cases for these values of t].

In eq. (1), $\mathbf{x}$ is the vector of state variables, x_i, defined by

$$\mathbf{x} \equiv [I, M, R, \lambda_0, \lambda_1, \lambda_2, \mu_0, \mu_1, \mu_2, T]^T \qquad (2)$$

and $\mathbf{u}$ is the vector of independent operating (or decision) variables, u_i. The following is the set of decision or control variables in this problem:

$$\mathbf{u} = [T_0^*, [I_0]^*, x_{\text{out}}^*, L_{x,\text{ini}}, T_w(t)]^T \qquad (3)$$

These variables can easily be changed in an experimental/industrial system and so comprise a reasonable set to use. These variables have to be *specified* ("givens" of the problem) so as to be able to evaluate the evolution of the state variables over time. In addition, these variables could be used in future optimization studies.

An additional complication present in the present problem is that the thickness, L_x, of the computational cell decreases with time. This makes this into what is referred to as the moving boundary problem. To obtain solutions to this problem, we simplify it and assume that the entire contents of any computational cell at time $t = 0$ and having an initial volume of $AL_{,\text{ini}}$ remain inside the cell of volume AL_x (having the *same* cross-sectional area, A) as the cell becomes thinner with time.

The PDEs in eq. (1) and Table V can be solved using the method of lines (finite differences).[17,18] This technique is used to convert the PDEs into a coupled set of several ODE–IVPs using the DSS002 code,[18] and the subroutine DIVPAG is then used to integrate the equations. The details of the numerical procedure

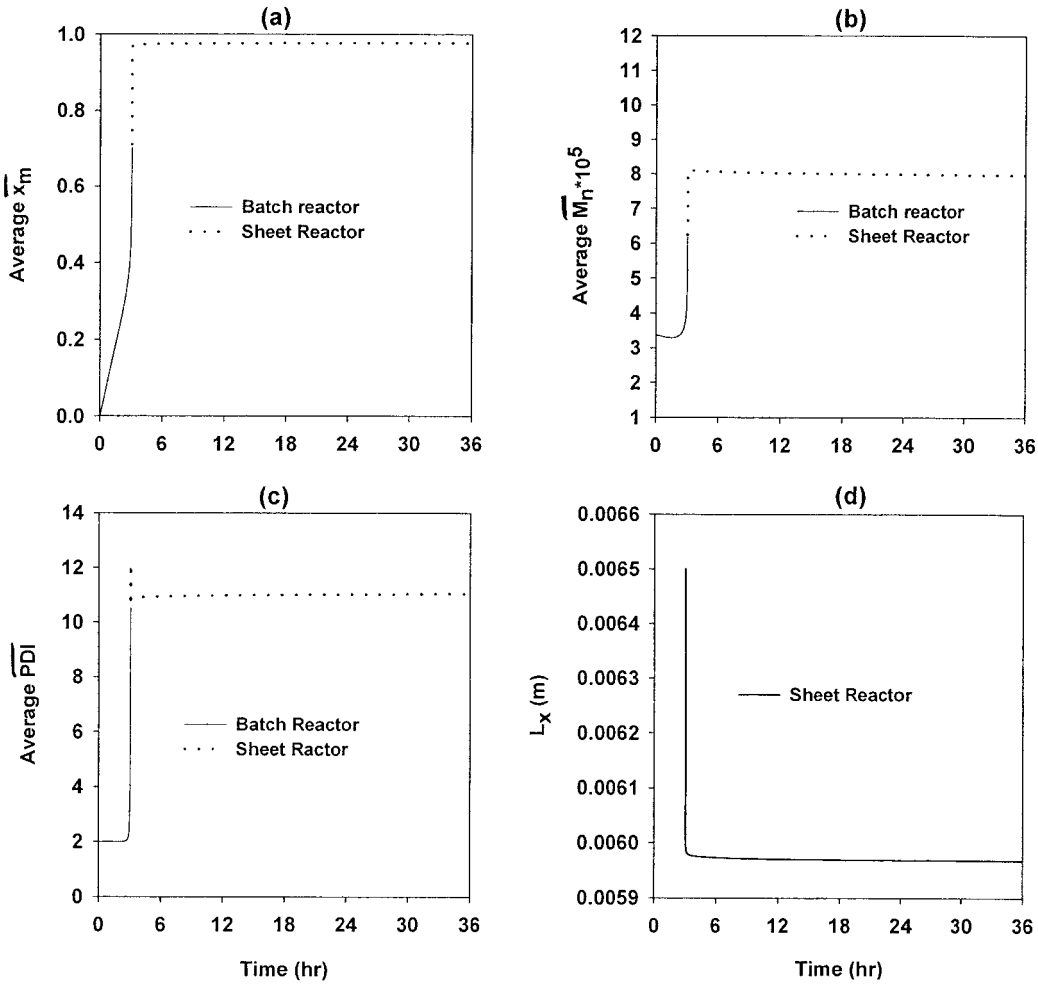

Figure 5 $\bar{x}_m$, $\bar{M}_n$, $\overline{\text{PDI}}$, and L_x as a function of t in the two reactors when $T_w(t)$ is constant at 55°C. Solid lines represent the batch reactor while dotted lines represent the sheet reactor.

used are now described: The domain, $0 \leq x \leq L_x$, at any time, t, is divided into $N + 1$ *equispaced* finite-difference grid planes (N cells of equal volume), as shown in Figure 2. The region between two consecutive grid planes, and having a cross-sectional area, A, is referred to as a finite-difference "cell." The reaction mixture in each finite-difference cell is assumed to polymerize during the short interval of time, $t \leq t \leq t + \Delta t$, at a temperature that is assumed to remain constant at the *instantaneous local* value, $T(x, t)$, for this short period. The volume of each finite-difference cell is, similarly, assumed to remain constant during this short interval of time and is (re-)computed at the end of the interval for each cell. Since the contraction of the volume would differ for each cell, the spacing of the grid planes would become unequal at time $t + \Delta t$, as polymerization progresses. Following the polymerization in cells having different thicknesses would lead to severe computational problems. Hence, at the end of each interval of time, we redistribute the $N + 1$ grid planes using an interpolation scheme (see Fig. A). The domain, $0 \leq x \leq L_x(t + \Delta t)$ is redivided at time $t + \Delta t$, into $N + 1$ new, equispaced grid planes. Obviously, the average values of T and of the concentrations and moments at (the center of each) finite-difference cell would change during this instantaneous operation of redistribution of the grid planes. The detailed procedure and equations for estimating the new interpolated values of all the variables during the redistribution are described in Table V.

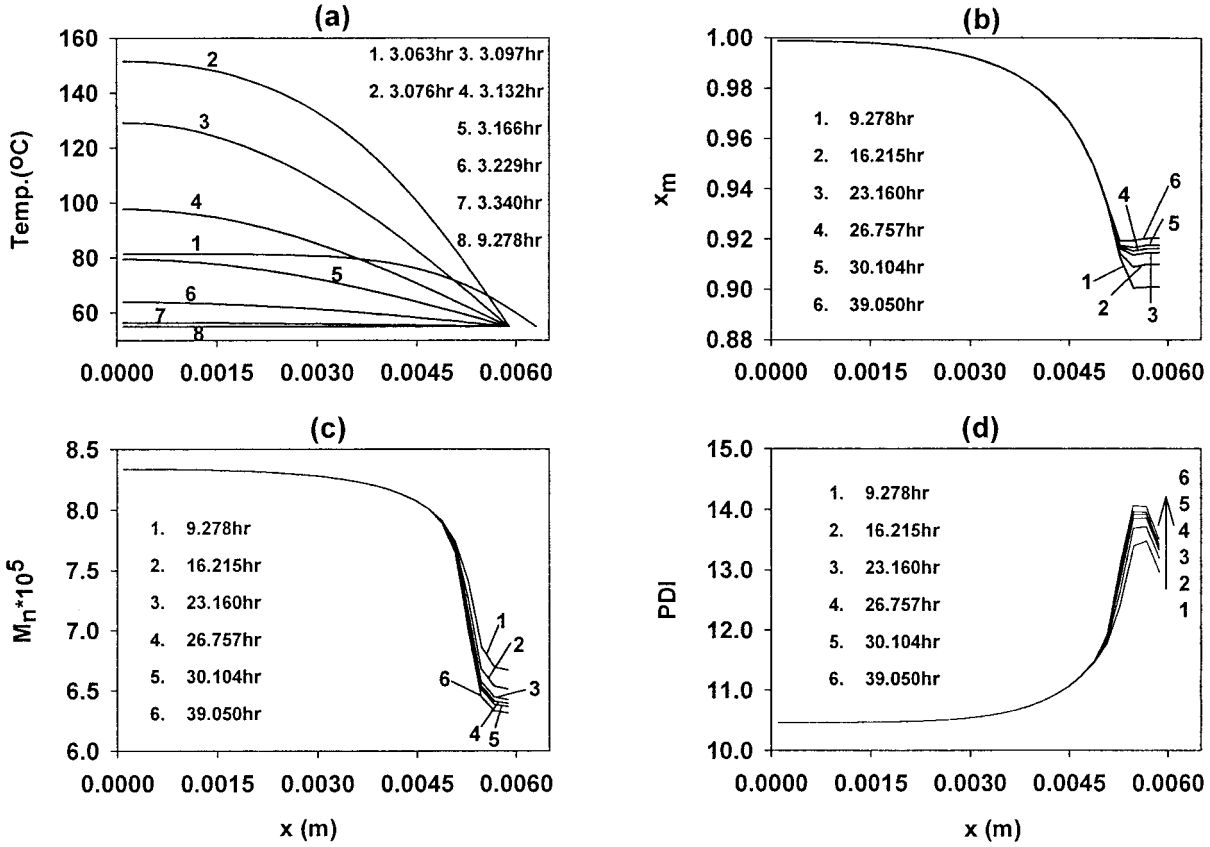

Figure 6 Variation of the local values of T, x_m, M_n, and PDI with x at different values of t. $T_w(t)$ constant at 55°C. $T(x)$ does not change any further for $t \leq 9.278$ h.

The entire set of *coupled* equations for each finite-difference cell are solved along with the equations in Table III for $t \leq t \leq t + \Delta t$. Thereafter, interpolation is carried out to obtain the new values of all the variables after the instantaneous redistribution of the grid planes. This procedure is repeated until the end of the sheet-casting process, $t = t_f$. At every interval, the section-average values of the monomer conversion ($\bar{x}_m$) and of the average molecular weights ($\bar{M}_n$ and $\bar{M}_w$) are evaluated using the expressions given in Table VI. The calculation of the local value of the monomer conversion (conversion in any finite-difference cell) is slightly difficult since we are unable to "define" an appropriate value of the "initial" moles of monomer in cell j because of the continuous redistribution of the grid planes. This is why we introduce a new variable, P_j, and keep updating it as the cell transforms due to the redistribution and interpolation procedures. P_j represents the mass of the polymer in cell j at any time. The "initial" number of moles of the monomer in cell j is, thus, simply the sum of M_j and $P_j/(MW_m)$. The monomer conversion in cell j is written as $1 - M_j/[M_j + (P_j/(MW_m)]$. In this study, the value of N was taken as 8, and it was confirmed that almost identical results were obtained when higher values of N (20, 30, or 40) were used.

RESULTS AND DISCUSSION

A computer code for the simulation of the entire process was written in FORTRAN 90 and tested extensively for errors. The code was then used to generate results for the following "reference" (ref) conditions of the decision variables :

$$T_0^* = 55°\text{C}$$

$$[I_0]^* = 22.0 \text{ mol/m}^3$$

$$x_{\text{out}}^* = 0.7$$

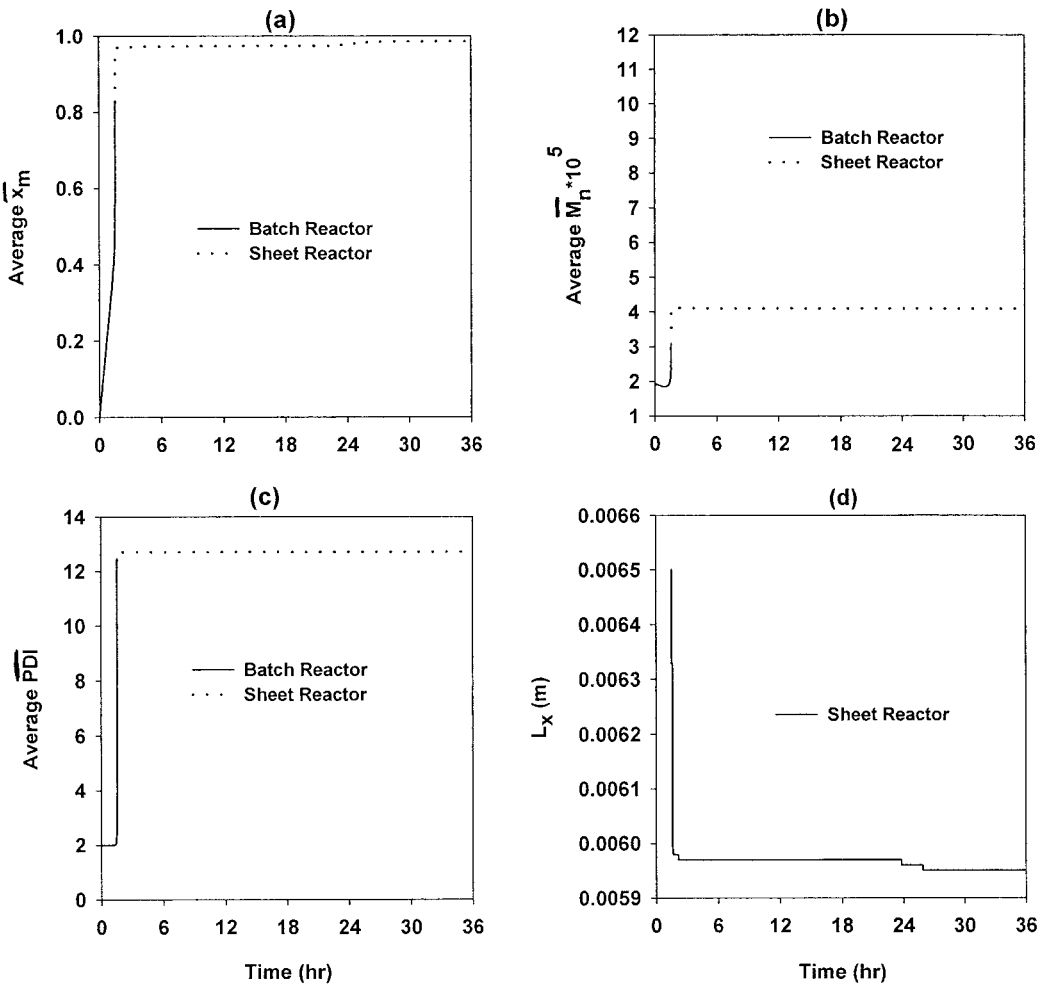

Figure 7 $\bar{x}_m$, $\bar{M}_n$, $\overline{\text{PDI}}$ and L_x as a function of t in the two reactors. $T_0^* = 65°C$. All other decision variables are at their reference values.

$$L_{x,\text{ini}} = 0.0065 \text{ m}$$

$$T_w(t): \text{ Table V} \tag{4}$$

The CPU time taken on an SGI Origin 2000 supercomputer for one such simulation run was 600 s.

Figure 3 shows the variations of the *section-average* values of the monomer conversion, $\bar{x}_m$, the number-average molecular weight, $\bar{M}_n$, and the polydispersity index, $\overline{\text{PDI}}$, as a function of time, t, for the reference conditions given in eq. (4). The solid curve represents the operation of the isothermal batch reactor at 55°C, while the dashed curve represents the sheet reactor under nonisothermal conditions. The variation of (half) the sheet thickness, L_x, with time is also shown.

Figure 4 shows the spatial variation of the *local* values of the temperature, monomer conversion, M_n, and PDI at different times in the sheet reactor. The variations of these variables, when the wall temperature in the sheet reactor is kept constant at 55°C all through the operation, are shown for comparison in Figures 5 and 6. The average conversion in the nonisothermal case is observed to be only very *slightly* larger, and the average molecular weight, slightly lower, near the end of the operation, after the wall temperature increases (after about 24 h). This is expected physically, since the increase of the temperature near the end of the operation reduces the difference between the polymerization and the glass transition temperatures (overcomes the glass effect to some extent) and so enables further poly-

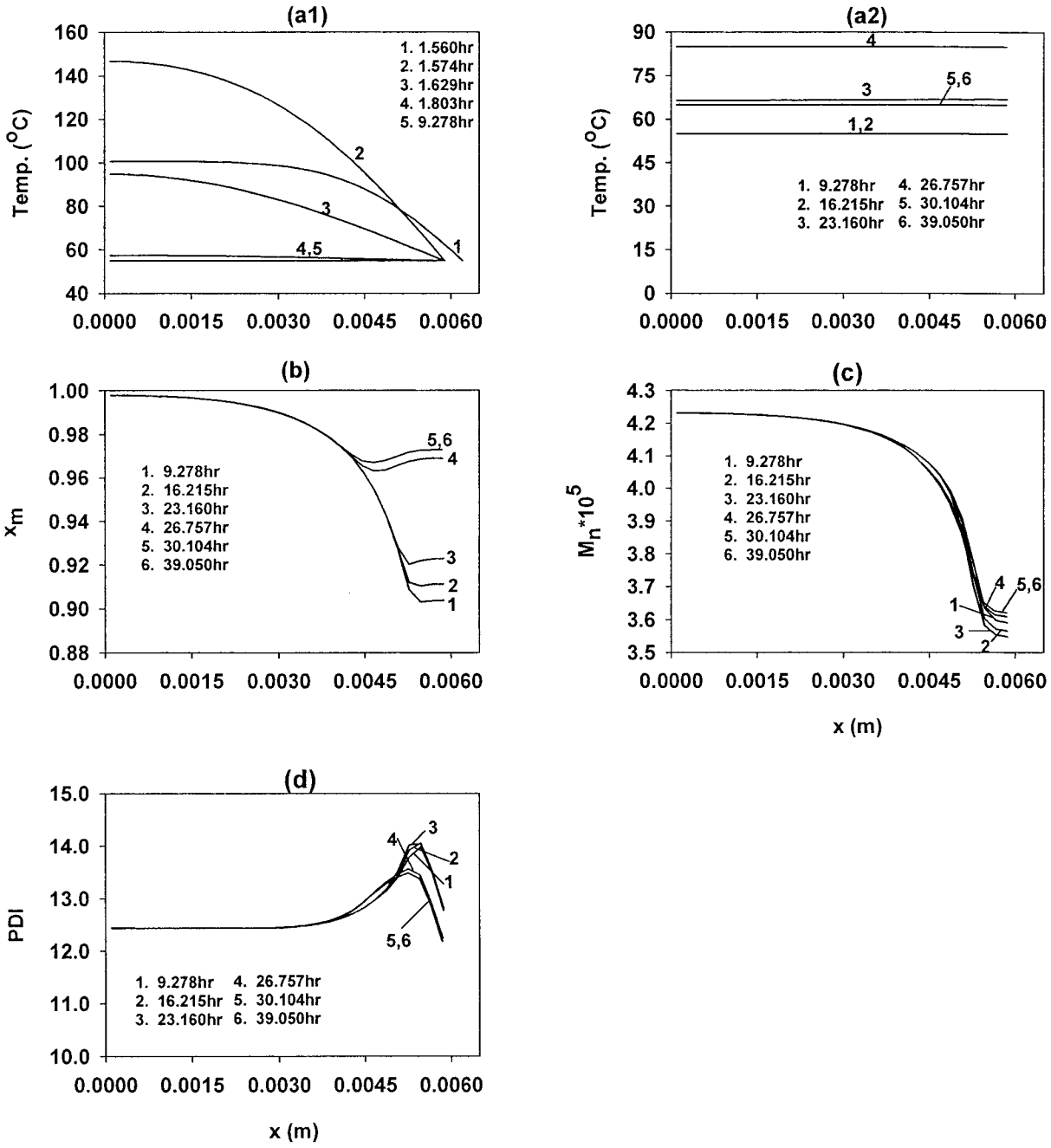

Figure 8 Local values of T, x_m, M_n, and PDI as a function of x at different values of t. $T_0^* = 65°C$. All other decision variables are at their reference values.

merization in the reference case. It is observed that the sheet thickness is smaller under nonisothermal conditions because of this additional polymerization.

An interesting phenomenon is observed when we compare the plots for the *local* values of the monomer conversion and the number-average molecular weights for the sheet reactor at different locations and times, both for the nonisothermal and the constant wall-temperature cases (Figs. 4 and 6). Even though there is no significant difference between the results for these two cases for M_n, it is found that the monomer conversion increases *dramatically* in the outer (oven-side)

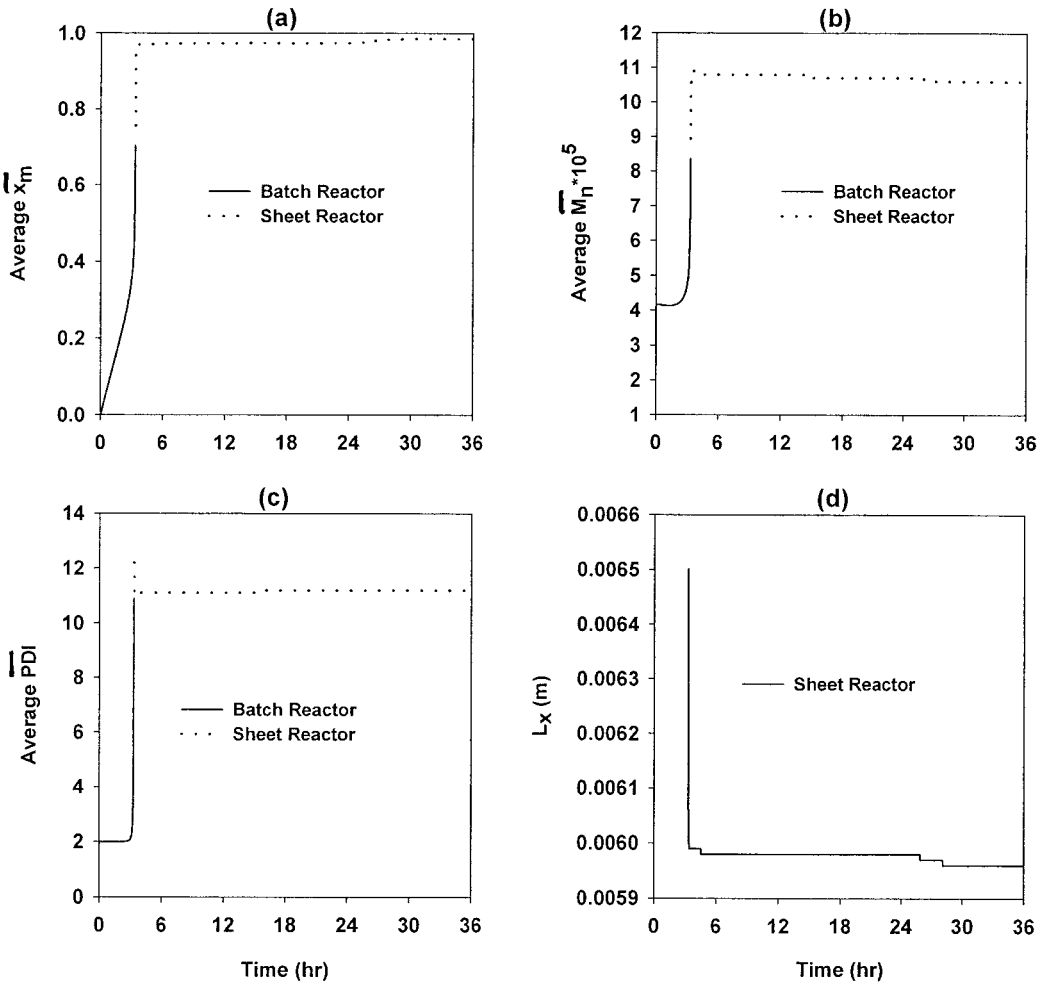

Figure 9 $\bar{x}_m$, $\bar{M}_n$, $\overline{\text{PDI}}$ and L_x as a function of t in the two reactors. $[I_0]^* = 15$ mol/m^3. All other decision variables are at their reference values.

region of the sheet from about 91 to about 97.5% in the case of nonisothermal operation. This, in fact, suggests why one uses temperature programming in this process. The exothermic nature of the polymerization leads to high temperatures (approxiately 150°C) near the center of the sheet during the early period of polymerization [Fig. 6(a); same $T(x)$ for $t \leq 20$ h for both isothermal and nonisothermal cases]. This leads to monomer conversions near unity in the central region (core). In contrast, the material near the wall experiences lower temperatures in the isothermal case, and so the monomer conversion in that region does not go above about 91%. The introduction of higher wall temperatures in the later stages of polymerization remedies this [see Fig. 4(a)] and leads to the formation of PMMA sheets that are stronger at the outer regions due to the attainment of higher monomer conversions there. Figures 4(d) and 6(d) show that the local values of PDI in the PMMA sheet are slightly lower in the nonisothermal case than when the operation is isothermal. This is again because of higher conversions in the nonisothermal case. In this case, too, as in the case of the average monomer conversion, the average value of the polydispersity index ($\overline{\text{PDI}}$) does not display any dramatic differences. Clearly, one has to study *local* rather *than section-average* values to understand reactor behavior. This insight can be of immense use in formulating appropriate optimization problems for this process in the future.

The effects of *a few* of the more important operating (decision) variables from among those listed in eq. (4), are now studied (other results can be supplied on request). These results can be compared with the reference results shown in Figures

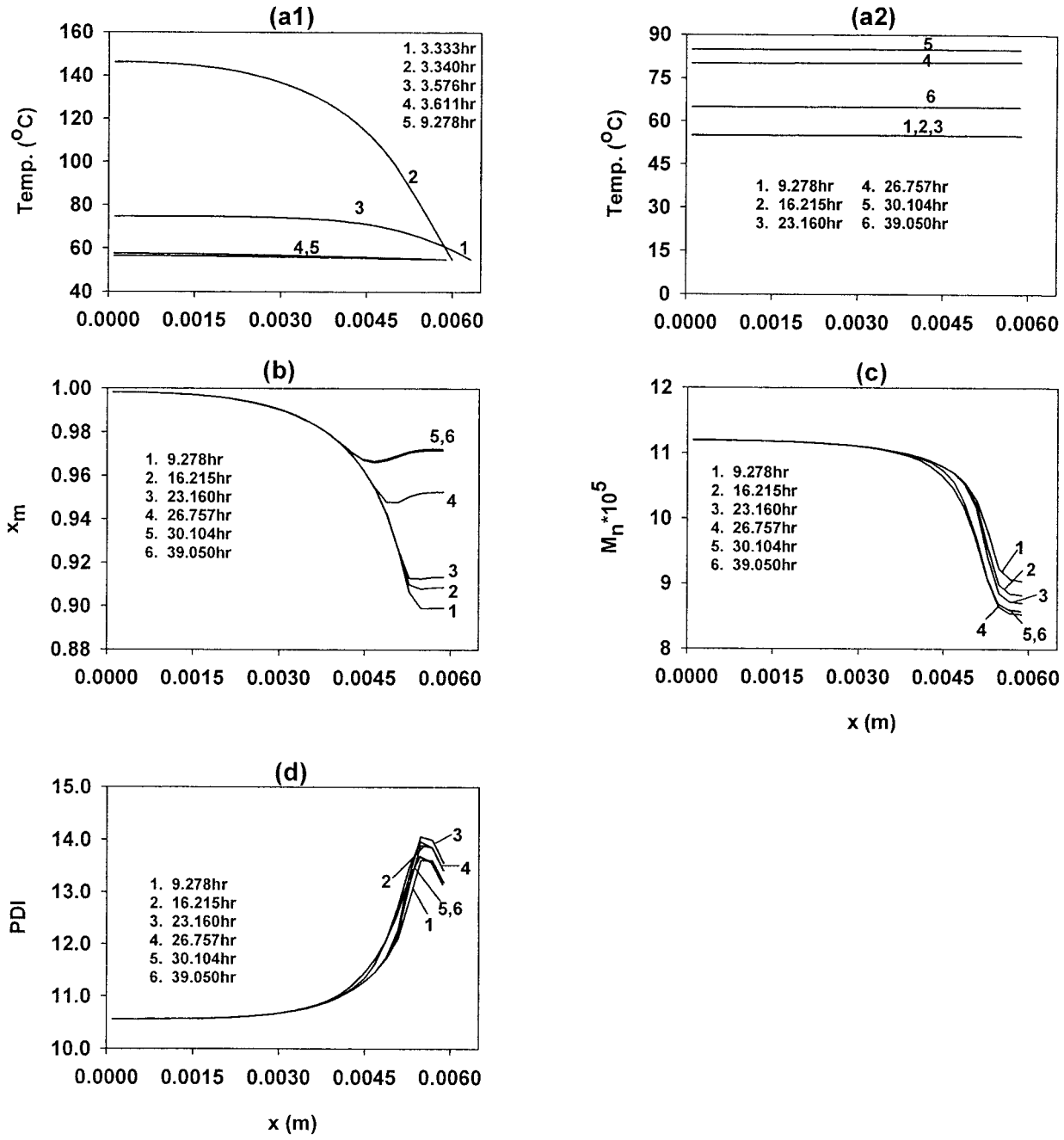

Figure 10 Local values of T, x_m, M_n, and PDI as a function of x at different values of t. $[I_0]^* = 15$ mol/m^3. All other decision variables are at their reference values.

3 and 4. Figures 7 and 8 show the effect of changing the temperature, T_0^*. This is the temperature of the isothermal batch reactor, as well as the wall temperature for the first 20 h in the sheet reactor and so is an important decision variable. Higher values of T_0^* speed up the reaction, but also lead to a significant lowering of the section-average value of the number-average molecular weight. The section-average value of the PDI is higher. These effects of temperature are expected for PMMA systems.

Figures 9 and 10 show the effect of a decrease in the initiator concentration, $[I_0]^*$, in the feed to the batch reactor from the reference value of 22 to

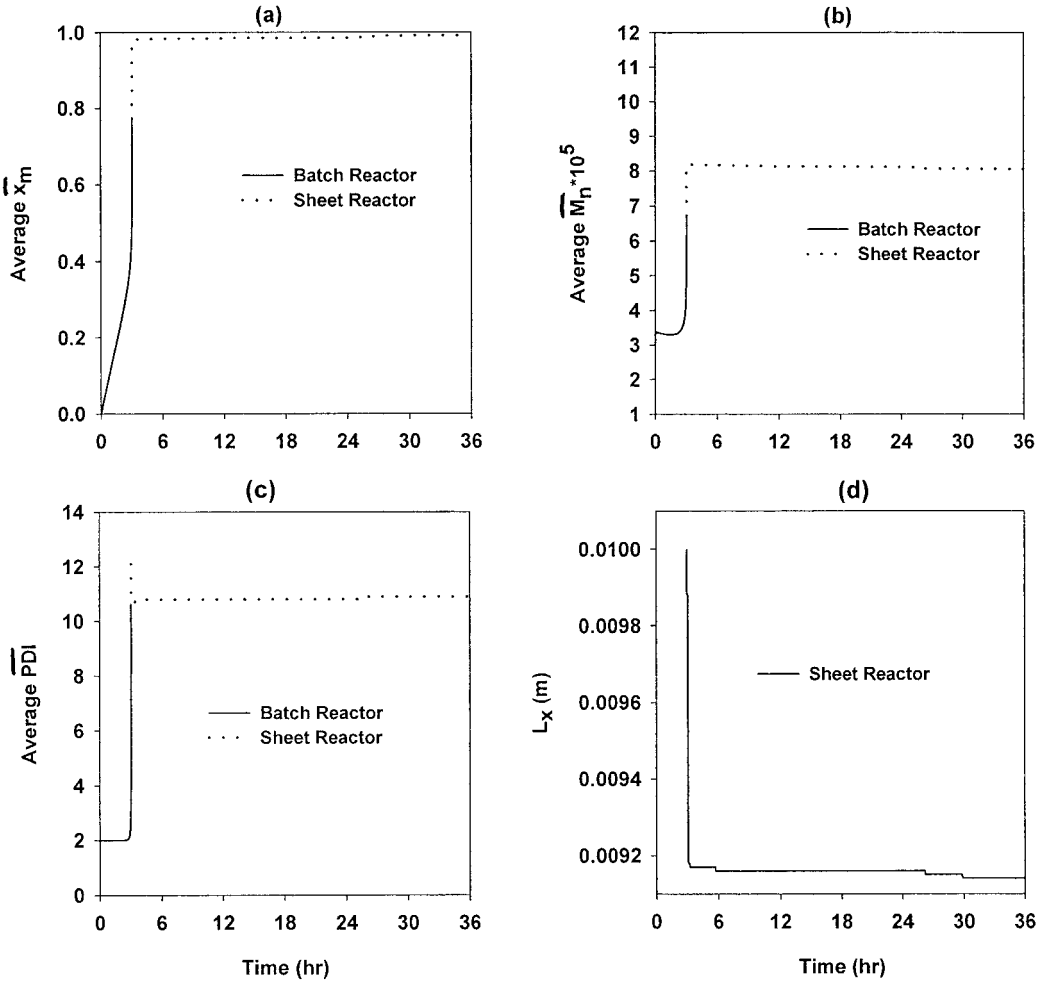

Figure 11 $\bar{x}_m$, $\bar{M}_n$, $\overline{\text{PDI}}$ and L_x as a function of t in the two reactors. $L_{,\text{ini}} = 0.01$ m. All other decision variables are at their reference values.

15 mol/m^3. It is clear that lower values of the initiator concentration lead to higher spatial-average values of M_n. This is expected physically, since lower initiator concentrations lead to lower concentrations of free radicals in the reaction mass and reduce the probability of termination. A similar effect is observed in Figure 10(c) which shows the variation of the local values of M_n. Figure 10 shows the variation of the local values of the monomer conversion and the PDI in the mold. The effects of the initiator concentration on these are small.

Figures 11 and 12 show the effect of increasing (half) the initial sheet thickness, $L_{,\text{ini}}$. As $L_{,\text{ini}}$ is increased, the heat-transfer resistance increases and temperatures in the inner core (at intermediate values of t) become higher, leading to higher values of the local monomer conversion (as well as its section-average value). The percent shrinkage is almost the same in both these cases (8.6% for $L_{,\text{ini}} = 0.01$ m compared to 8.4% for the reference case).

Figures 13 and 14 show the effect of changing $T_w(t)$, the wall-temperature history. Only one parameter characterizing the function, $T_w(t)$, is changed—the highest temperature, $T_{w,\max}$, from 85 to 90°C during 24 h $\leq t \leq$ 27 h. Obviously, the rate of increase or decrease of $T_w(t)$ during 20 h $\leq t \leq$ 24 h and 27 h $\leq t \leq$ 28 h (Table V) are higher. The most important influence of this is that higher local values of the monomer conversion are achieved near the walls.

Figures 15 and 16 show the effect of reducing x^*_{out}, the monomer conversion at the end of the batch reactor, to 0.3. The Trommsdorff effect is manifested *almost entirely* inside the mold in this

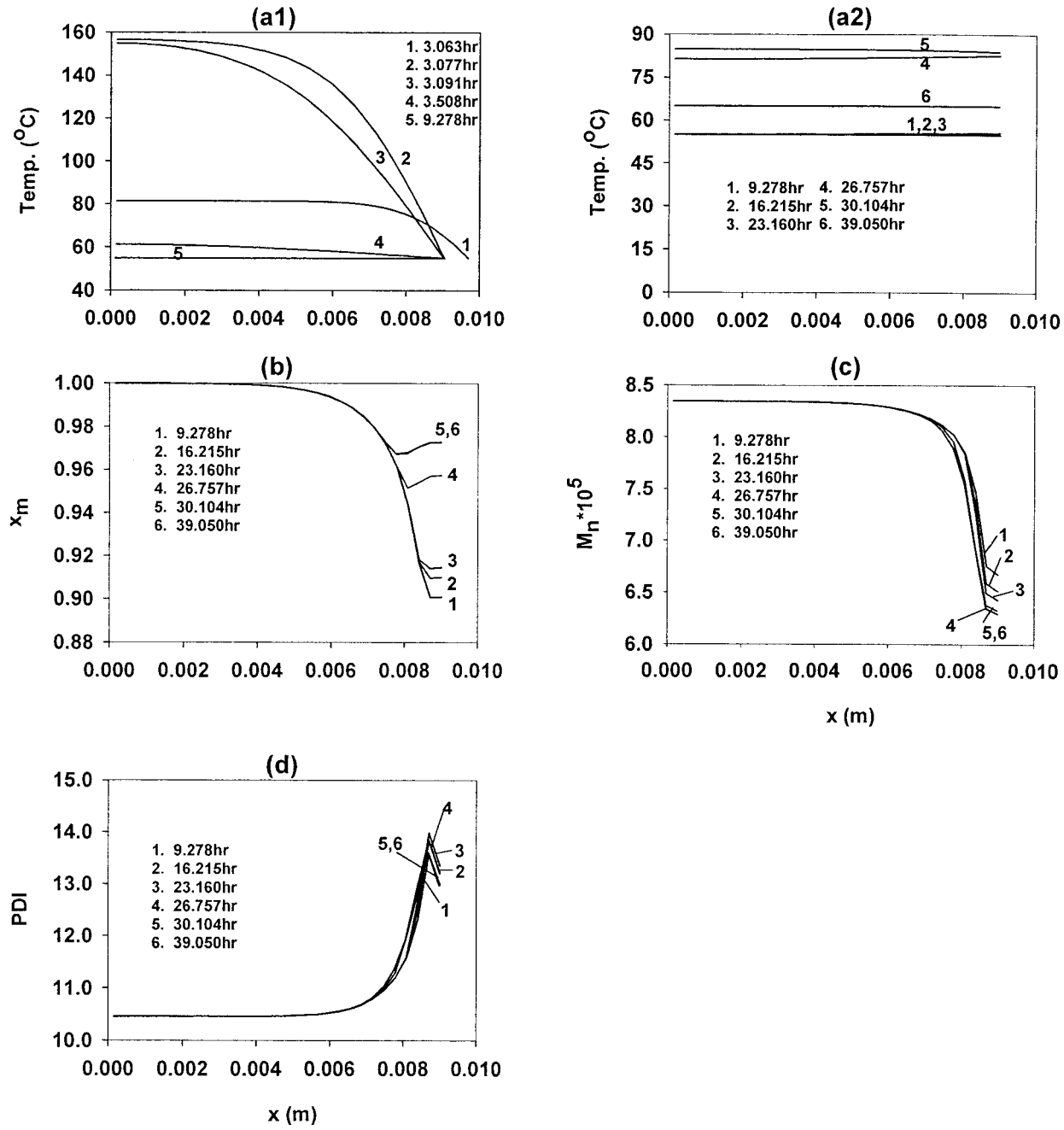

Figure 12 Local values of T, x_m, M_n, and PDI as a function of x at different values of t. $L_{,\text{ini}} = 0.01$ m. All other decision variables are at their reference values.

case (in the reference case, where x^*_{out} was 0.7, part of this effect occurred in the batch reactor). The temperature history experienced by the reaction mass is obviously different in this case, and because of this, higher values of the local and section-average values of the monomer conversion (and, so, slightly thinner PMMA sheets) are obtained. Interestingly, the section-average value of the number-average molecular weight is slightly higher, but the section-average value of the PDI is much lower in this case. These would have considerable influence on the properties of the final product. This is an interesting inference and can be useful in optimization studies as well.

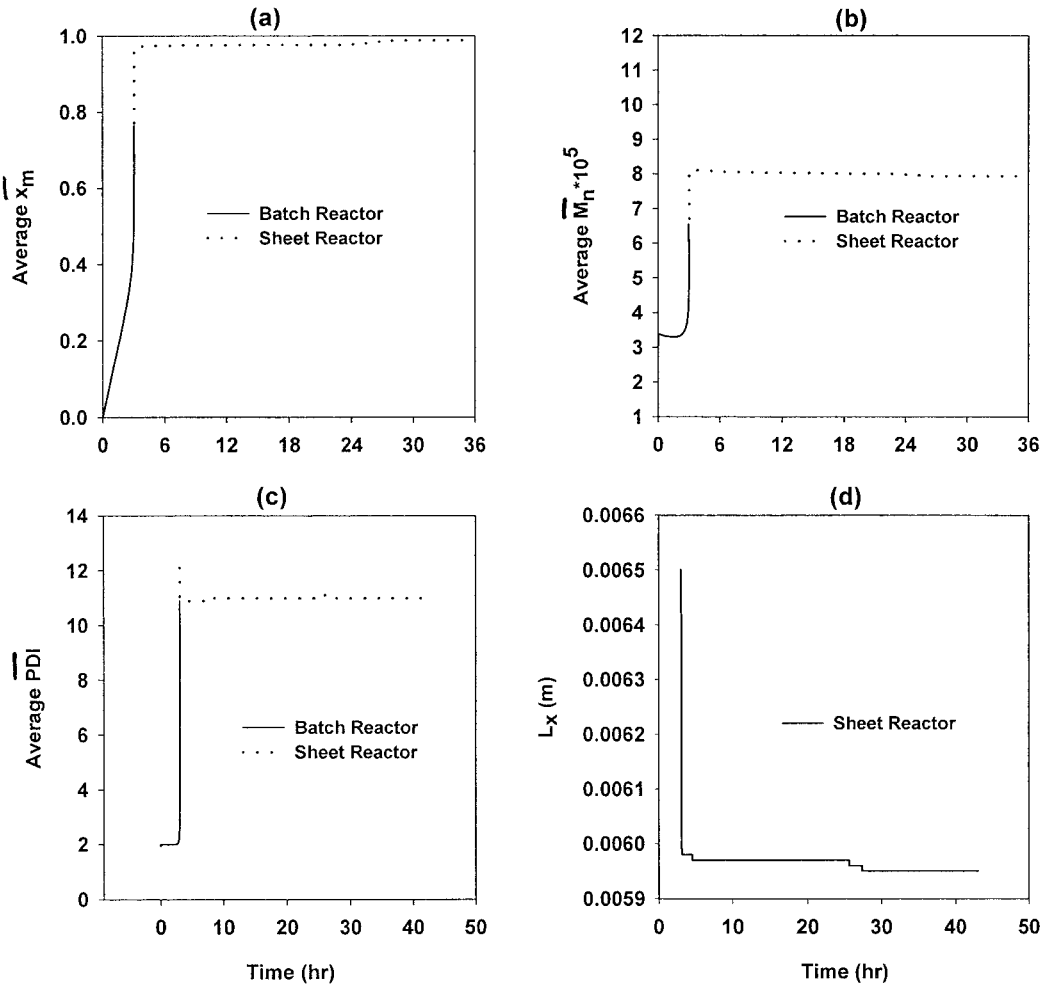

Figure 13 $\bar{x}_m$, $\bar{M}_n$, $\overline{\text{PDI}}$ and L_x as a function of t in the two reactors. $T_{w,\max} = 90°C$ during 24 h $\leq t \leq$ 27 h in the sheet reactor. All other decision variables are at their reference values.

CONCLUSIONS

A model was developed for the sheet molding of MMA. Some interesting observations were made regarding the influence of temperature programming in the furnace on the *local* values of the monomer conversion *in a thin region near the walls* of the mold. The insights developed herein could be useful in optimization studies of this operation.

NOMENCLATURE

A	cross-sectional area of the sheet reactor (m^2)
$C_{p,\text{mix}}$	specific heat of the reaction mixture in the sheet reactor (J kg^{-1} K^{-1})
D_n	dead polymer molecule having n repeat units
E_d, E_p, E_t	activation energies for the reactions in Table I (kJ/mol)
f	initiator efficiency
f_0	Initiator efficiency in the limiting case of zero diffusional resistance
$-\Delta H_r$	enthalpy of the propagation reaction (J/mol)
I^*	moles of initiator in the batch reactor at any time, t (mol)

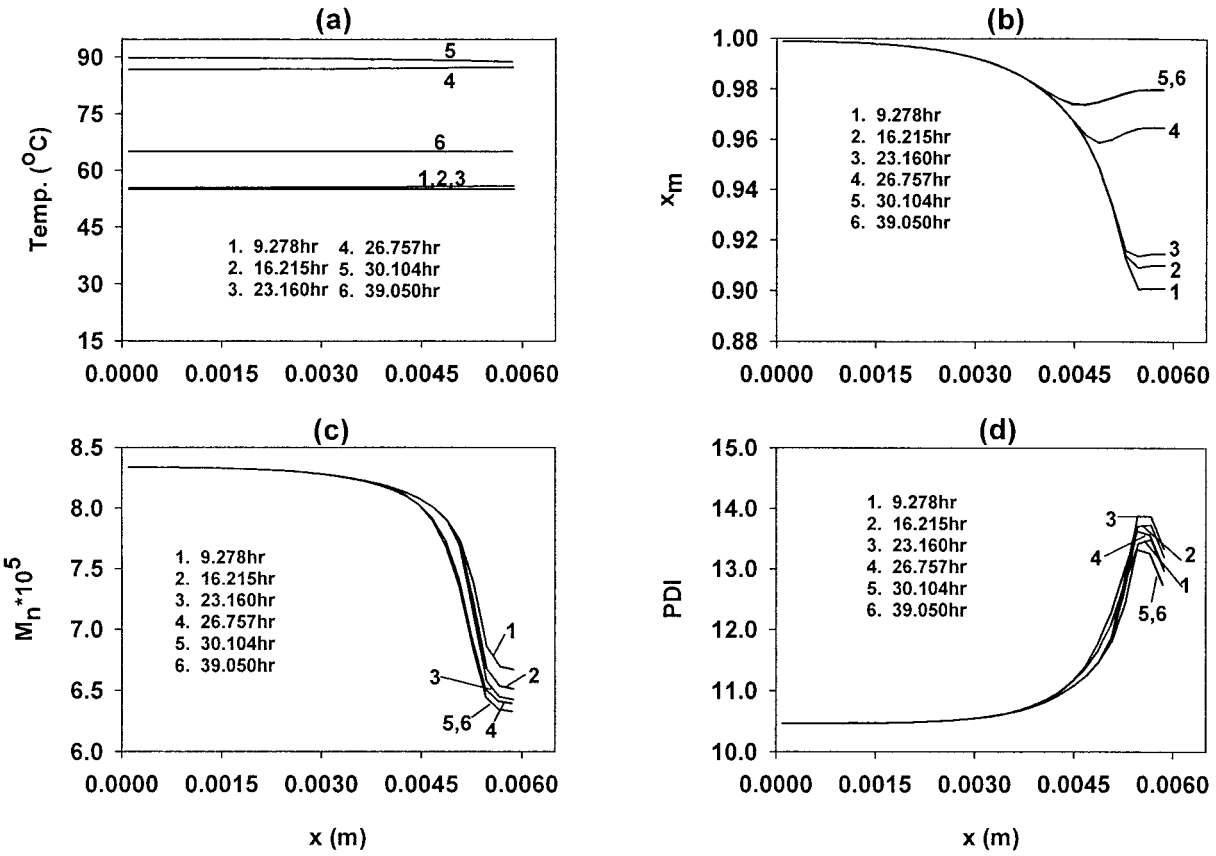

Figure 14 Local values of T, x_m, M_n, and PDI as a function of x at different values of t. $T_{w,\max} = 90°C$ during 24 h $\leq t \leq$ 27 h in the sheet reactor. All other decision variables are at their reference values.

$[I_0]^*$ molar concentration of initiator in feed of batch reactor (mol/m^3)

I_j moles of initiator in any cell, j, in the sheet reactor at time t (mol)

k_d, k_i, k_p, k_t rate constants for initiation, propagation, and termination in the presence of the gel and glass effects (1/s, or m^3 mol^{-1} s^{-1})

$k_{i,0}$, $k_{p,0}$, $k_{t,0}$ intrinsic (in absence of cage, gel, and glass effects) rate constants (m^3 mol^{-1} s^{-1})

k_d^0, $k_{p,0}^0$, $k_{t,0}^0$ frequency factors for intrinsic rate constants (1/s or m^3 mol^{-1} s^{-1})

K_T thermal conductivity of the reaction mixture in the film reactor (W m^{-1} K^{-1})

L_x half the sheet thickness at time t (m)

M^* moles of monomer in the batch reactor at time t (mol)

M_0^* "initial" moles of monomer corresponding to cell, j, in the sheet reactor after regridding, at time t (mol)

M_j moles of monomer in cell, j, in the sheet reactor at time t (mol)

M_{jp} molecular weight of the polymer jumping unit (kg/mol)

$M_{n,j}$ number-average molecular weight $[= (\text{MW}_m)\,(\lambda_1 + \mu_1)/(\lambda_0 + \mu_0)]_j$ in cell, j, in the sheet reactor at time t (kg/mol)

$M_{w,j}$ weight-average molecular weight $[= (\text{MW}_m)\,(\lambda_2 + \mu_2)/(\lambda_1 + \mu_1)]_j$ in cell, j, in the sheet reactor at time t (kg/mol)

(MW_I), (MW_m) molecular weights of pure primary radicals and monomer (kg/mol)

N number of cells in the sheet reactor

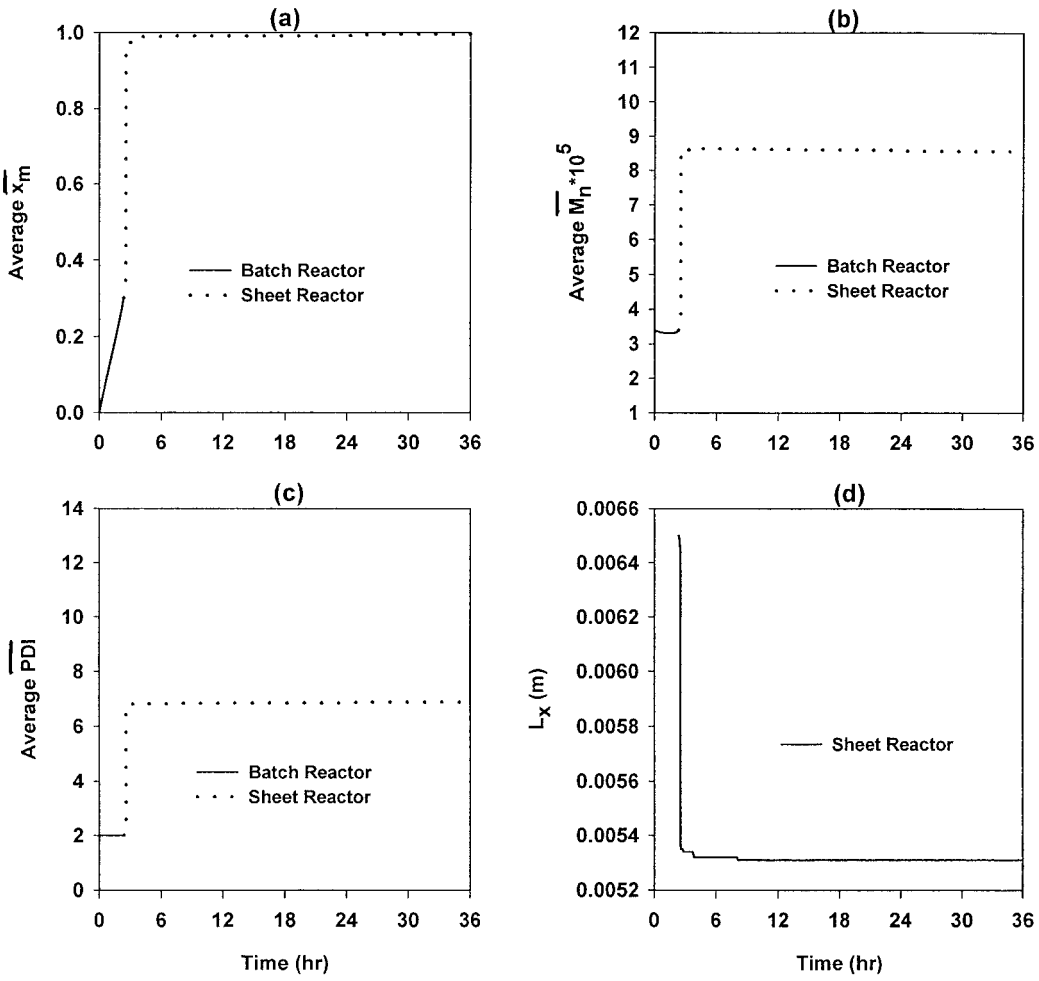

Figure 15 $\bar{x}_m$, $\bar{M}_n$, $\overline{\text{PDI}}$ and L_x as a function of t in the two reactors. $x^*_{\text{out}} = 0.3$. All other decision variables are at their reference values.

P_n growing polymer radical having n repeat units

P_j mass of polymer in cell, j, in the sheet reactor at time t (kg)

PDI_j polydispersity index in cell, j, in the sheet reactor at time t

R^* moles of primary radicals in the batch reactor at time t^*(mol)

R_j moles of primary radicals in cell, j, in the sheet reactor at time t (mol)

R_g universal gas constant (kJ mol^{-1} K^{-1})

t reaction time in the batch reactor (h)

t reaction time in the sheet reactor [$t = 0$ at start of polymerization in the mold] (h)

Δt time interval (s)

T temperature of the reaction mixture in cell, j, in the sheet reactor at time t (K)

T^* temperature of the isothermal batch reactor (K)

V^* volume of reaction mixture in the batch reactor at time t^*(m^3)

V_j volume of reaction mixture in cell, j, in the sheet reactor at time t (m^3)

V_{fm}, V_{fp} free volume of monomer and polymer

$\hat{V}^*_I$, $\hat{V}^*_{m,}$ $\hat{V}^*_p$ specific critical hole free volumes of initiator, monomer, and polymer (m^3/kg)

x transverse location in the sheet reactor from the center line (m)

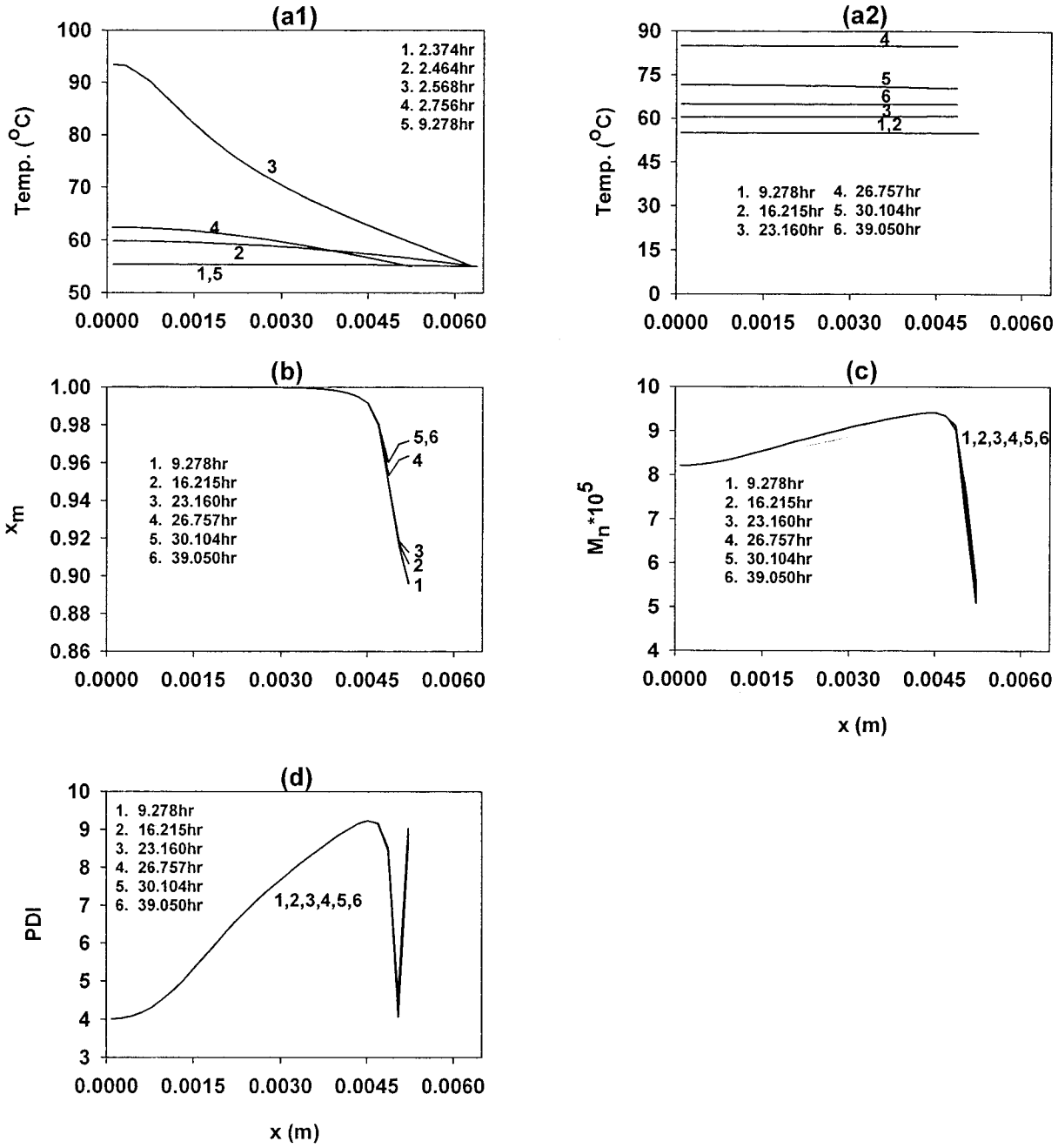

Figure 16 Local values of T, x_m, M_n, and PDI as a function of x at different values of t. $x^*_{\text{out}} = 0.3$. All other decision variables are at their reference values.

Δx_j thickness of cell, j, in the sheet reactor at time t (m)

x^*_m monomer conversion in the batch reactor at time t^*

$x_{m,j}$ local monomer conversion in cell, j, in the sheet reactor at time t

Greek Letters

γ overlap factor

ξ_{13}, ξ_{I3} ratio of the molar volume of the monomer and initiator jumping unit to the critical molar volume of the polymer, respectively

θ_f, θ_p, θ_t parameters in the model for the cage, gel, and glass effects, respectively (m^3/mol, s, s)

λ_k^* kth (k = 0, 1, 2, . . .) moment of live polymer radicals, P_n, in the batch reactor at time t^* (mol)

μ_k^* kth (k = 0, 1, 2, . . .) moment of dead polymer radicals, D_n, in the batch reactor at time t^* (mol)

$\lambda_{k,j}$ kth (k = 0, 1, 2, . . .) moment of live polymer radicals, P_n, in cell, j, in the sheet reactor at time t (mol)

$\mu_{k,j}$ kth (k = 0, 1, 2, . . .) moment of dead polymer radicals, D_n, in cell, j, in the sheet reactor at time t (mol)

μ_n number-average chain length

ρ_m, ρ_p densities of pure (liquid) monomer and of pure polymer [functions of temperature only] (kg/m^3)

ϕ_m, ϕ_p volume fractions of monomer and polymer in the reaction mass

Subscripts/Superscripts

ini starting value in the sheet reactor

f final value (at $t = t_f$) at the end of the sheet reactor

new values after instantaneous redistribution of the grid planes in the sheet reactor

0 feed to the batch reactor

out product of the batch reactor

w wall of the sheet reactor

* values in the batch reactor

Symbols

$\overline{\ldots}$ cross-section average (over $0 \leq x \leq L_x$) in the sheet reactor at time t

REFERENCES

1. Beattie, J. O. Mod Plast 1969, 46, 684.
2. Trommsdorff, V. E.; Kohle, H.; Lagally, P. Makromol Chem 1947, 1, 169.
3. Norrish, R. G. W.; Smith, R. R. Nature 1942, 150, 336.
4. Chiu, W. Y.; Carratt, G. M.; Soong, D. S. Macromolecules 1983, 16, 348.
5. Achilias, D. S.; Kiparissides, C. J Appl Polym Sci 1988, 35, 1303.
6. Achilias, D. S.; Kiparissides, C. Macromolecules 1992, 25, 3739.
7. Seth, V.; Gupta, S. K. J Polym Eng 1995, 15, 283.
8. Gao, J.; Penlidis, A. J Macromol Sci-Rev Macromol Chem Phys 1996, 36, 199.
9. Mankar, R. B.; Saraf, D. N.; Gupta, S. K. Ind Eng Chem Res 1998, 37, 2436.
10. Zhou, F. B.; Gupta, S. K.; Ray, A. K. J Appl Polym Sci 2000, 78, 1439.
11. Chakravarthy, S. S. S.; Saraf, D. N.; Gupta, S. K. J Appl Polym Sci 1997, 63, 529.
12. Garg, S.; Gupta, S. K. Macromol Theory Simul 1999, 8, 46.
13. Ray, A. B.; Saraf, D. N.; Gupta, S. K. Polym Eng Sci 1995, 35, 1290.
14. Vargaftik, N. B. Handbook of Thermal Conductivity of Liquids and Gases; CRC: Boca Raton, FL, 1994.
15. H. F.; Mark, Bikales, N. M.; Overberger, C. G.; Menges, G. Encyclopedia of Polymer Science Engineering, 2nd ed.; Wiley: New York, 1986; Vol. 4.
16. Louie, B. M.; Soong, D. S. J Appl Polym Sci 1985, 30, 3707.
17. Gupta, S. K. Numerical Methods for Engineers; New Age International: New Delhi, 1995.
18. Schiesser, W. E. The Numerical Method of Lines; Academic: New York, 1991.